外部電場の作用する半導体超格子における量子コヒーレンス

大阪市立大学工学部　　福尾　　毅
東北大学理学部　　　　小川　哲生
大阪市立大学工学部　　中村　勝弘

（日本語要旨）

　近年の半導体レーザーや微小共振器加工技術の進展に伴い、光の量子論的理解が急速に進んでいる。とりわけ、スクイーズド光に代表される光の非古典状態は、最小不確定状態にありながら、一方の正準共役量の揺らぎが従来のコヒーレント光よりも小さく、量子光通信や高精度測定などへの応用が期待されている。そのような非古典光を生成する場合、これまでは主に非線型光学媒質を用いて実験が行われ、その内部での電子系と光子場の相互作用がブラックボックスとして取り扱われてきた。

　一方、MBEに代表される近年の半導体微細加工技術の発展により、結晶中の電子状態を人工的に制御できるようになった。異なる種類の半導体超薄膜の周期積層構造である半導体超格子に対して電場を加えた場合、ブロッホ振動と呼ばれる電子の往復運動が生じ、THzオーダーの光源として光物性の分野では盛んに研究されている。

　本研究ではそのブロッホ振動によって種々の光、とりわけ非古典光の生成が可能であることを示唆し、それらの光子場量子状態は外部電場という１つのパラメーターによって制御されうることを明らかにした。また、半導体超格子中における電子のダイナミクスがいかにして光子場に影響を及ぼし、そして非古典光が生成されるかについても詳細に述べる。

Quantum Coherence in Semiconductor Superlattices with External dc Bias

Tsuyoshi Fukuo

Department of Applied Physics, Osaka City University, Sugimoto, Sumiyoshi-ku, Osaka 558, Japan

Tetsuo Ogawa

Department of Physics, Tohoku University, Aoba-ku, Sendai 980-77, Japan

Katsuhiro Nakamura

Department of Applied Physics, Osaka City University, Sugimoto, Sumiyoshi-ku, Osaka 558, Japan

Abstract

We show that the Bloch oscillation in semiconductor superlattices under the external dc bias is able to generate nonclassical photon states. On the single-subband condition, the time development operator of the photon field in such systems is obtained and is shown to be equivalent approximately to the displacement operator, the quadrature-phase amplitude squeezing operator, or the optical Kerr operator, depending on the external dc bias. Such equivalence is discussed in terms of Wannier-Stark ladder formation. The effects of intersubband transition of electrons are also investigated.

1 Introduction

Generation and control of quantum states of light have been extensively studied recently, and, in particular, the quadrature-phase amplitude (QPA) squeezed state and/or the photon-number squeezed state have attracted a considerable interest among engineers in application areas as well as fundamental researchers. So far, such states have been generated by using optical nonlinear susceptibilities [1].

On the other hand, a rapid progress in fabrication of nanoscale structures has made it possible to see typical quantum-mechanical effects such as ballistic transport and tunneling. In particular, a growing attention has been paid to superlattices with an alternating sequence of potential barriers and wells.

In this Paper, we investigate the time development of the quantized electromagnetic field (photon field) in superlattices under the external dc bias and show quantum-mechanically that the Bloch oscillation is able to emit coherent radiation. Specifically, it is revealed that the system can also emit nonclassical light, say QPA squeezed light and/or photon-number squeezed light, which can be controlled by the modulation of the external dc bias.

This Paper is organized as follows. In Sec. 3.2, after a brief review of Bloch oscillation we introduce the interaction Hamiltonian between quantized photon field and electrons in semiconductor superlattice. Section 3.3 is devoted to the analytical calculation of the time development operators for several cases of external dc field. Effects of intersubband transition are studied in Sec. 3.4.

2   What is Bloch oscillation?

2.1   Acceleration theory

We consider the tight-binding Hamiltonian of conduction electrons in semiconductor superlattice with a periodicity d, which consists of $(2N + 1)$ quantum-wells. In the presence of electric field $E(t)$, such Hamiltonian is given by

$$\hat{\mathcal{H}}(t) = \sum_{m=-N}^{N} \left\{ [\Delta_0 + meE(t)d]\, \hat{b}_m^\dagger \hat{b}_m - \frac{\Delta_1}{4} \left(\hat{b}_m \hat{b}_{m+1}^\dagger + \hat{b}_{m+1} \hat{b}_m^\dagger \right) \right\}. \tag{1}$$

$\hat{b}_m$ $(\hat{b}_m^\dagger)$ is the annihilation (creation) operators in a well m; the first term gives the (field-dependent) site energies and the second term describes hopping to nearest-neighbor wells. Here, we have prescribed Δ_0 and Δ_1 as the energy of the isolated quantum-well state and four times the nearest-neighbor interaction energy, respectively. In this Section, we assume that the gap energy between subbands is so large that the excitations to higher subbands can be neglected.

In the absence of electric field, we can easily diagonalize the Hamiltonian Eq. (1) as

$$\hat{\mathcal{H}}(k) = \sum_k \epsilon(k) \hat{b}_k^\dagger \hat{b}_k, \tag{2}$$

with eigenenergies

$$\epsilon(k) = \Delta_0 - \frac{\Delta_1}{2} \cos(kd), \tag{3}$$

under the Fourier transformations

$$\begin{cases} \hat{b}_m &= \frac{1}{\sqrt{2N+1}} \sum_k e^{-imkd}\hat{b}_k \\ \hat{b}_m^\dagger &= \frac{1}{\sqrt{2N+1}} \sum_k e^{imkd}\hat{b}_k^\dagger \end{cases} , \tag{4}$$

where k is the wave number along the superlattice axis. Equation (3) gives a quasicontinuous energy spectrum corresponding to a subband dispersion as shown in Figs. 1(a) and (b).

In the presence of an electric field $E(t)$, the translational symmetry of a superlattice potential is broken, and the Bloch electron in the superlattice shows a striking behavior, say Bloch oscillation [2, 3] in both the wave number and real space according to the so-called acceleration theorem [4]:

$$k(t) = k_0 + \frac{eA(t)}{\hbar} = k_0 - \frac{e \int dt E(t)}{\hbar}, \tag{5}$$

where k_0 and $A(t)$ are an initial wave number and a component of vector potential along the superlattice axis, respectively. Equation (5) is also available from Newton's kinetic equation $d(\hbar k)/dt = -eE(t)$. We can introduce the pseudo-wave number in Eq. (5) unless the electric field is strong enough to collapse the subband picture. Using the Fourier transformations

$$\begin{cases} \hat{b}_m &= \frac{1}{\sqrt{2N+1}} \sum_{k(t)} e^{-imk(t)d}\hat{b}_{k(t)} \\ \hat{b}_m^\dagger &= \frac{1}{\sqrt{2N+1}} \sum_{k(t)} e^{imk(t)d}\hat{b}_{k(t)}^\dagger \end{cases} , \tag{6}$$

as well as Eq. (4), the Hamiltonian in the presence of electric field is rewritten as

$$\begin{aligned} \hat{\mathcal{H}}(t) &= \sum_{k(t)} \left\{ \Delta_0 - \frac{\Delta_1}{2} \cos[k(t)d] \right\} \hat{b}_{k(t)}^\dagger \hat{b}_{k(t)} \\ &= \sum_{k_0} \left\{ \Delta_0 - \frac{\Delta_1}{2} \cos[k(t)d] \right\} \hat{b}_{k_0}^\dagger \hat{b}_{k_0}. \end{aligned} \tag{7}$$

The time-dependent Hamiltonian in Eq. (7) is diagonalized at each instant of time in the Hilbert space of accelerated wave number in Eq. (5). Since the electric field E, regardless of its time-dependence or independence, *accelerates* electrons in a subband homogeneously, the electrons with different initial wave numbers k_0 never catch up with each other. So we can use the accelerated wave number states as an instantaneous bases.

Because the Bloch oscillation leads to a THz oscillator device emitting a coherent electromagnetic radiation, its phenomenon has been intensively studied theoretically and experimentally in recent years [7].

2.2 Model and Hamiltonian

The electric field operator in our system (see Fig. 2) is described by

$$\hat{E}(t) = E_0 + iE_1 \left(\hat{a}e^{-i\omega t} - \hat{a}^\dagger e^{i\omega t} \right), \tag{8}$$

where the first term E_0 represents the external dc bias and the second term represents the quantized photon field. In Eq. (8), E_1 is the electric field per photon, ω is the frequency of the alternating field, and $\hat{a}$ ($\hat{a}^\dagger$) is the photon annihilation (creation) operator. (In this Paper we shall consider only a single-mode quantized field.) Using Eq. (8) in Eq. (5), we find the accelerated wave number, and, substituting it into the dispersion relation Eq. (7), we can obtain the time-dependent Hamiltonian

$$\hat{\mathcal{H}}(t) = \sum_{k_0} \left\{ \Delta_0 - \frac{\Delta_1}{2} \cos \left[k_0 d - \Omega_{B0} t + \frac{\Omega_{B1}}{\omega} \left(\hat{a}e^{-i\omega t} + \hat{a}^\dagger e^{i\omega t} \right) \right] \right\} \hat{b}^\dagger_{k_0} \hat{b}_{k_0}, \tag{9}$$

where Ω_{B0} and Ω_{B1} are the characteristic frequencies defined as $\Omega_{B0} \equiv eE_0 d/\hbar$ and $\Omega_{B1} \equiv eE_1 d/\hbar$, respectively. Specifically, we obtain the photon Hamiltonian by employing the independent electron picture and choosing a $k_0 = 0$ state [8],

$$\hat{\mathcal{H}}(t) = -\frac{\Delta_1}{2} \cos \left[\Omega_{B0} t - \frac{\Omega_{B1}}{\omega} \left(\hat{a}e^{-i\omega t} + \hat{a}^\dagger e^{i\omega t} \right) \right]. \tag{10}$$

(Here we neglect the constant term Δ_0.) As mentioned above, the electrons in a subband do not interact with each other, say, the initial wave number k_0 is a good quantum number. So the assumption of a choice of k_0 electronic state holds without loss of generality.

The Hamiltonian in Eq. (10) describes the interaction between a Bloch electron in dc biased superlattice and the single-mode quantized photon field. Since the photon field operators are contained in the Hamiltonian nonlinearly, we can expect various optical nonlinear effects. It is difficult to treat this Hamiltonian exactly. Therefore we employ some approximations as follows:

$$\hat{\mathcal{H}}(t) \approx -\frac{\Delta_1}{4} \left\{ e^{i\Omega_{B0}t} - \frac{\Omega_{B1}^2}{2\omega^2} \left[\hat{a}^2 e^{i(\Omega_{B0}-2\omega)t} + \left(2\hat{a}^\dagger \hat{a} + 1 \right) e^{i\Omega_{B0}t} + \hat{a}^{\dagger 2} e^{i(\Omega_{B0}+2\omega)t} \right] \right.$$
$$\left. + \frac{\Omega_{B1}}{i\omega} \left[\hat{a}e^{i(\Omega_{B0}-\omega)t} + \hat{a}^\dagger e^{i(\Omega_{B0}+\omega)t} \right] \right\} + \text{H.c.} \tag{11}$$

Here, we had recourse to the second-order Taylor expansion in Ω_{B1}/ω. Because we confine ourselves to the case of THz-order frequency ω ($\Omega_{B1} \ll \omega$), the expansion is justified.

3 Time development operator: analytical results

Now, we shall have the time development operator

$$\hat{U}(t) = \mathrm{T}\left\{\exp\left[-\frac{i}{\hbar}\int_0^t dt'\hat{\mathcal{H}}(t')\right]\right\}, \tag{12}$$

by using Hamiltonian in Eq. (11). All information about the temporal evolution of the photon field is contained in the operator $\hat{U}(t)$. As pointed out by some previous papers [5, 6], the matching ratio between Ω_{B0} and ω plays an important role in the temporal evolution of the system. In the following, we shall concentrate on some interesting matching ratios with which $\hat{U}(t)$ can be calculated analytically by resorting to the rotating-wave approximation (RWA).

The $\Omega_{B0} = \omega$ *case*: We apply RWA to Eq. (12), say, neglect the terms which has the oscillatory time dependence (e.g., $\hat{a}^\dagger e^{i(\Omega_{B0}+\omega)t}$) because their contributions are averaged out in the time integral. As a result, the time development operator is reduced to

$$\hat{U}(t) = \exp(\alpha\hat{a}^\dagger - \alpha^*\hat{a}), \tag{13}$$

where

$$\alpha = -\frac{\Delta_1}{4\hbar}\frac{\Omega_{B1}}{\omega}t. \tag{14}$$

The operator corresponds to the displacement operator $\hat{D}(\alpha)$ in quantum optics [1], which leads the initial vacuum state $|0\rangle$ to the coherent state $|\alpha\rangle$. So the mean photon number of the quantized photon field is amplified and coherent radiation with frequency Ω_{B0} is emitted from the vacuum state. The amplification is due to the resonance effect between Bloch oscillation frequency Ω_{B0} and cavity frequency ω.

We can also interpret this correspondence by the concept of Wannier-Stark ladder formation [7]. Figure 3(a) shows the schematic diagram of the real-space energy state of electron in dc biased superlattice. The localized electron can move through the superlattice due to the tunneling to the nearest-neighbor quantum-well and subsequent transition via photon emission (or absorption) with energy $\hbar\Omega_{B0}$. So the Hamiltonian of the system is given by

$$\hat{\mathcal{H}} = \frac{\Delta_1}{4}\frac{\Omega_{B1}}{\omega}i\left(\hat{a} - \hat{a}^\dagger\right), \tag{15}$$

with the resultant time development operator rewritten as in Eq. (13).

The $\Omega_{B0} = 2\omega$ *case*: When $\Omega_{B0} = 2\omega$ is satisfied, the contributions of the terms except for $\hat{a}^2 e^{i(\Omega_{B0}-2\omega)}$ and $\hat{a}^{\dagger 2} e^{-i(\Omega_{B0}-2\omega)}$ are averaged out in the time integral. As a result, the time development operator is given by

$$\hat{U}(t) = \exp\left(\frac{1}{2}\xi^*\hat{a}^2 - \frac{1}{2}\xi\hat{a}^{\dagger 2}\right), \tag{16}$$

where

$$\xi = i\frac{\Delta_1}{4\hbar}\left(\frac{\Omega_{B1}}{\omega}\right)^2 t. \tag{17}$$

The operator corresponds to nothing but the QPA squeezing operator $\hat{S}(\xi)$ in quantum optics, which leads the initial coherent state to the QPA squeezed state. When the nonlinear optical process such as four-wave mixing is used to generate the QPA squeezed light, the powerful pump beam, which can be treated classically, is needed [1]. In our scheme, the external dc bias plays such a role. And, similarly to the $\Omega_{B0} = \omega$ case, we can also interpret this correspondence by using the concept of Wannier-Stark ladder formation as in Fig. 3(b). The localized electron can move in the superlattice due to the tunneling to the nearest-neighbor well and subsequent transition by two-photon emission (or absorption) with energy $\hbar\Omega_{B0}/2$. So the Hamiltonian of the system is given by

$$\hat{\mathcal{H}} = \frac{\Delta_1}{4}\frac{1}{2!}\left(\frac{\Omega_{B1}}{\omega}\right)^2\left(\hat{a}^2 + \hat{a}^{\dagger 2}\right), \tag{18}$$

with the time development operator rewritten as in Eq. (16).

Generally, when $\Omega_{B0} = m\omega$ is satisfied with positive integer m, the contributions of the terms except for the $\hat{a}^m e^{i(\Omega_{B0}-m\omega)}$ and $\hat{a}^{\dagger m} e^{-i(\Omega_{B0}-m\omega)}$ are averaged out in the time integral, and the time development operator is calculated as

$$\hat{U}(t) = \exp\left[i\frac{\Delta_1}{2\hbar}\frac{\left(\frac{\Omega_{B1}}{\omega}\right)^m}{m!}\frac{\hat{a}^m e^{-i\frac{\pi}{2}m} + \hat{a}^{\dagger m} e^{i\frac{\pi}{2}m}}{2}t\right]. \tag{19}$$

The modulation of the external dc bias lets us control the energy spacing between nearest-neighbor quantum-wells, and it leads to the m-photon transition.

In the $\Omega_{B0} = 0$ *case*: This condition corresponds to the case that the external dc bias E_0 is absent. When we apply the RWA to the Hamiltonian Eq. (11), the terms proportional to $\hat{a}^{\dagger}\hat{a}$ (and constant terms) are left alone, which do not affect the temporal evolution of the photon field. So we shall expand the trigonometric functions up to a higher-order

Table 1: Classification of generated quantized photon states.

External dc bias	Corresponding unitary operator $\hat{U}(t)$	Generated quantized photon states
$\Omega_{B0} = \omega$	$\hat{D}(\alpha) \equiv \exp(\alpha\hat{a}^\dagger - \alpha^*\hat{a})$	Coherent state
$\Omega_{B0} = 2\omega$	$\hat{S}(\xi) \equiv \exp\left(\frac{1}{2}\xi^*\hat{a}^2 - \frac{1}{2}\xi\hat{a}^{\dagger 2}\right)$	QPA squeezed state
$\Omega_{B0} = 0$	$\hat{U}_{\mathrm{K}}(\gamma) \equiv \exp\left(\frac{i}{2}\gamma\hat{a}^{\dagger 2}\hat{a}^2\right)$	Photon-number squeezed state

(concretely, up to the fourth-order) term and neglect $\hat{a}^\dagger\hat{a}$ (and constant) terms. In such a case, the time development operator is available as

$$\hat{U}(t) = \exp\left(\frac{i}{2}\gamma\hat{a}^{\dagger 2}\hat{a}^2\right), \tag{20}$$

where

$$\gamma = \frac{\Delta_1}{4\hbar}\left(\frac{\Omega_{B1}}{\omega}\right)^4 t. \tag{21}$$

This unitary operator corresponds to the optical Kerr operator $\hat{U}_{\mathrm{K}}(\gamma)$ discussed by Kitagawa and Yamamoto [9], who showed that this yields photon-number squeezing. The Hamiltonian they discussed consists of a four-photon process of the single-mode quantized photon field, and the similar process can be expected to occur in the superlattice.

When the external dc bias is absent, the potential shape of the superlattice is affected by the quantized photon field itself and it is *tilted* alternately as schematically shown in Fig. 3(c). The electron transferred via tunneling to the nearest-neighbor quantum-well would experience the subsequent transition. However, the energy levels are alternately shifted upward or downward. So we can interpret that the transitions by photon emission and photon absorption occur in the same quantum-well site. If we expand the trigonometric functions up to the fourth-order, the fourth-order (the second-order) term corresponds to *two-photon absorption and two-photon emission* (*one-photon absorption and one-photon emission*). The fourth-order term gives the Hamiltonian term proportional to $\hat{a}^{\dagger 2}\hat{a}^2$, and it corresponds to the Kerr-like interaction.

Table I summarizes the generated quantized photon states mentioned above.

4 Intersubband transition

In this Section, we shall investigate the effect of the intersubband transition of electron(s) to consolidate the results obtained in the previous Section.

We consider the tight-binding model of a two-subband system, written as

$$
\hat{\mathcal{H}}(t) = \sum_{m=-N}^{N} \left\{ \left[\Delta_0^b + meE(t)d \right] \hat{b}_m^\dagger \hat{b}_m - \frac{\Delta_1^b}{4} \left(\hat{b}_m \hat{b}_{m+1}^\dagger + \hat{b}_{m+1} \hat{b}_m^\dagger \right) \right.
$$
$$
\left. + \left[\Delta_0^c + meE(t)d \right] \hat{c}_m^\dagger \hat{c}_m + \frac{\Delta_1^c}{4} \left(\hat{c}_m \hat{c}_{m+1}^\dagger + \hat{c}_{m+1} \hat{c}_m^\dagger \right) + V(t) \left(\hat{b}_m \hat{c}_m^\dagger + \hat{c}_m \hat{b}_m^\dagger \right) \right\}.
$$
$$\tag{22}$$

Here the first (second) two term give the lower (upper) subband tight-binding Hamiltonian, and last term is the one responsible for the on-site intersubband transfer. ($V(t)$ is the matrix element dependent on the electric field $E(t)$).

This Hamiltonian does neglect the transition matrix elements between different sites, but it contains the essential physics for the problem [10]. Note that the hopping parameters of upper and lower subbands are written with opposite signs because of the difference in the parity between corresponding localized Wannier functions in each of isolated quantum-well states.

The Hamiltonian Eq. (22) can be also written in terms of accelerated wave number basis by resorting to the Fourier transformation Eq. (6), that is,

$$
\hat{\mathcal{H}}(t) = \sum_{k_0} \left(\left\{ \Delta_0^b - \frac{\Delta_1^b}{2} \cos\left[k(t)d \right] \right\} \hat{b}_{k_0}^\dagger \hat{b}_{k_0} + \left\{ \Delta_0^c + \frac{\Delta_1^c}{2} \cos\left[k(t)d \right] \right\} \hat{c}_{k_0}^\dagger \hat{c}_{k_0} \right.
$$
$$
\left. + V(t) \left[\hat{b}_{k_0} \hat{c}_{k_0}^\dagger + \hat{c}_{k_0} \hat{b}_{k_0}^\dagger \right] \right).
$$
$$\tag{23}$$

By introducing the independent particle picture as well as Eq. (10) and putting $\Delta_0^b = \Delta_0^c$, we can reduce Eq. (23) to

$$
\hat{\mathcal{H}}(t) = \frac{1}{2} \left\{ \Delta_0 - \frac{\Delta_1}{2} \cos\left[\Omega_{B0}t - \frac{\Omega_{B1}}{\omega} \left(\hat{a}e^{-i\omega t} + \hat{a}^\dagger e^{i\omega t} \right) \right] \right\} \hat{S}_z + V(t) \left(\hat{S}_- + \hat{S}_+ \right), \tag{24}
$$

where, $\hat{S}_z, \cdot \hat{S}_-$, and $\hat{S}_+$ are Pauli pseudo-spin operators. Equation (24) is analogous to the so-called Jaynes-Cummings (JC) model, which describes the interaction between the discrete two-levels of an atom and quantized photon field [1, 12]. Instead of eigenstates

corresponding to discrete levels, however, we consider two-subbands of semiconductor superlattice which have quasicontinuous spectrum. Furthermore, the matrix element of intersubband transition $V(t)$ is given as follows:

$$
\begin{aligned}
V(t) = \hbar \Big[& g_0 + g_1 \left(\hat{a} e^{-i\omega t} + \hat{a}^\dagger e^{i\omega t} \right) + g_2 \left(\hat{a}^2 e^{-2i\omega t} + \hat{a}^{\dagger 2} e^{2i\omega t} \right) \\
& + g_3 \left(\hat{a}^3 e^{-3i\omega t} + \hat{a}^{\dagger 3} e^{3i\omega t} \right) + ... \Big],
\end{aligned}
\tag{25}
$$

where the first term describes zero photon transition via dc bias (Zener tunneling), the second one does a single photon transition, and the left ones correspond to multi-photon transitions. Because we now consider the subbands which have quasicontinuous spectrum unlike the discrete spectrum in atomic level, various (linear- and nonlinear-) transition process are possible and all of them are contained in Eq. (25). In the following, we calculate quantities numerically by using Hamiltonian Eq. (24) and approximations shown in Eq. (11) to discuss the intersubband transition.

We make no attempt in this Section to evaluate the coefficients $g_{0,1,2,3,...}$ from the first principle, since we are interested in the consideration of not quantitative but qualitative effects of intersubband transition on the results obtained in previous Section (single-subband condition). And to make the effect clearer, we set the coefficients much greater than their real values estimated from typical superlattice parameters.

4.1 Transition via photoabsorption (-emission)

First, we investigate the effects of intersubband transition via photoabsorption (or emission). On such a viewpoint, the matching ratio between Δ_0 (separation of subband midpoints) and $\hbar\omega$ (energy of a photon) is expected to play an important role as conjectured from the analogy with JC model.

Figures 4(a) and (b) show the temporal evolution of the mean photon-number $\langle \hat{n} \rangle$ in the case $\Omega_{\mathrm{B0}} = \omega$ with $\Delta_0/\hbar\omega = $ integer and $\Delta_0/\hbar\omega \neq$ integer, respectively. (In the following calculations, we include up to triple photon transitions in Eq. (25).) Comparing these figures, one finds that the mean photon-number is suppressed (worse amplifier) under the resonance condition in Fig. 4(a). This results can be interpreted as follows: The photon field prepared in vacuum state $|0\rangle$ is amplified by corresponding displacement operator Eq. (13) on condition that $\Omega_{\mathrm{B0}} = \omega$ is satisfied, as led in Eq. (13). The displacement direction in phase-space is decided by the phase of complex number α, proportional to the

hopping energy Δ_1. As already mentioned, the phase of Δ_1 is different by π between lower and upper subbands due to the symmetry of the localized Wannier functions. Thus the displacement directions are opposite with each other so that they are counteracted and the mean photon number is not amplified very much in case of Fig. 4(a). Unlike this, in Fig. 4(b), an electron is *localized* in lower subband almost all the time, since the matching ratio $\Delta_0/\hbar\omega$ is out of resonance and the transition to the upper subband is suppressed. It leads to the displacement in one direction in phase-space and the amplifier works effectively. In Fig. 5, maximal value of mean photon-number is plotted as a function of matching ratio $\hbar\omega/\Delta_0$. This figure also shows that if the resonant condition $\Delta_0/\hbar\omega = $ integer is satisfied, effectiveness of amplifier is decreased.

Figures 6(a) and (b) show the temporal evolution of the QPA variance $\langle\Delta\hat{q}^2\rangle$ in the $\Omega_{B0} = 2\omega$ case for $\Delta_0/\hbar\omega = $ integer and $\Delta_0/\hbar\omega \neq $ integer respectively. Comparing these figures, one finds that the QPA variance becomes larger (worse squeezing) under the resonant condition Fig. 6(a). And, similarly to the $\Omega_{B0} = \omega$ case (Fig. 4), we can also interpret this results as follows: An electron experiences the QPA squeezing in the phase-space under the condition $\Omega_{B0} = 2\omega$, and the direction is decided by the phase of complex number ξ given in Eq. (17). The squeezing direction in the upper subband is orthogonal to the one in the lower subband because of the phase difference by π between these pair of subbands. So, in the resonance case of Fig. 5(a), the QPA squeezing is suppressed with a large probability of the intersubband transition. In Fig. 7, the minimal value of QPA variance is plotted as a function of matching ratio $\hbar\omega/\Delta_0$. This figure shows that if the resonant condition $\Delta_0/\hbar\omega = $ integer is satisfied, squeezing effect is weakened.

In general, the intersubband transition counteracts the contributions of individual subbands summarized in Table 1, if the two-subband have opposite curvature. So we need to take the parameter values which forbid the intersubband transition such as $\Delta_0/\hbar\omega \neq $ integer, for the purpose of achieving the quantized photon states caused by the single subband condition.

We here make a comment on the existing works which treated the alternating field classically [5, 6, 13]. In those papers, analytic formulas for dynamical localization and intersubband Rabi oscillation were derived, from which resonant transition between quasienergy bands were revealed. Whereas, we have treated the ac field as quantized photon field together with an approximation of truncating Taylor expansion in the second-order in

Eq. (11). This approximation is effective in investigating the dynamics of quantized photon field. The neglected higher-order terms correspond to the tilt with the ac field, and striking products such as the quasienergy bands and the dynamical localization can not be introduced under the approximation. So the necessary condition to yield the higher probabilities of intersubband transition is slightly different from the one given in [6] and becomes

$$\Delta_0 \approx i\hbar\omega + j\hbar\Omega_{B0}, \tag{26}$$

with positive integer i and j. A laborious calculation gives the expression for the Hamiltonian avaraged over time including the effects of the higher-order terms:

$$
\begin{aligned}
\langle \hat{\mathcal{H}}(t) \rangle_t &\equiv \frac{1}{2\pi} \int_0^{2\pi} dt \hat{\mathcal{H}}(t) \\
&= -\frac{\Delta_0}{4} e^{(\Omega_{B1}/\omega)^2/2} \sum_{s=0}^{\infty} \left[\frac{(-i\Omega_{B1}/\omega)^{m+2s}}{s!(s+m)!} \hat{a}^{m+s} \hat{a}^{\dagger\,s} + \frac{(i\Omega_{B1}/\omega)^{m+2s}}{s!(s+m)!} \hat{a}^s \hat{a}^{\dagger\,s+m} \right],
\end{aligned}
\tag{27}
$$

with $\Omega_{B0} = m\omega$. Replacement of the creation and annihilation operators by c-number amplitudes $\sqrt{n}$ yield the quasienergy spectrum proportional to Bessel function

$\epsilon = -(\Delta_0/2) J_m (2\sqrt{n}\Omega_{B0}/\omega)$.

4.2   Zener tunneling

In the case of multiple-bands system with an applied dc electric field, it is well known that the dc field adds an essential new feature to the dynamics of carriers, say, Zener tunneling [3]. Rotvig *et al.* have studied coherent transport of one-dimensional semiconductor superlattices within two-subbands model [14]. They found that coherent oscillation between the subbands can occur at special values of the applied field, where there are avoided crossings of the two interpenetrating Wannier-Stark ladders arising from essentially different bands.

Fig. 8(a) shows the temporal evolution of the electronic inversion $\langle \hat{S}_z \rangle$, that is, the population difference between upper and lower subbands, when only the dc field is tuned to the resonant coupling between Wannier-Stark states without including the quantized ac field in Eqs. (24) and (25). We can see the stable plateaus corresponding to the Bloch oscillation and *instantaneous bursts* due to the Zener tunneling at the zone boundaries. In

Fig. 8(b), maximal value of electronic inversion is plotted as a function of matching ratio $\hbar\Omega_{B0}/\Delta_0$. This figure shows that, if the resonant condition

$$\Delta_0 \approx j\hbar\Omega_{B0} \tag{28}$$

is satisfied for a positive integer j, complete population inversion can be accomplished. The condition corresponds to the case aligning adjacent Wannier-Stark states in quantum wells j lattice spacing apart, in the Wannier-Stark ladder picture. They are referred to jth Zener resonance.

Furthermore, by setting proper parameters, we can observe the competition between two kinds of intersubband transition: photoabsorption (or emission) transition and Zener tunneling in the time domain. If the initial state for quantized photon field (electron) is prepared in vacuum states (lower subband), an electron can not absorb photon and the intersubband transition via photoabsorption is prohibited. On the contrary, Zener tunneling to the upper subband is allowed regardless of the photon states so long as the resonance condition Eq. (28) is satisfied. So, the early stage of the temporal evolution, Zener tunneling dominates the intersubband transition as shown in Fig. 9(a). In Fig. 9(b), temporal evolution of mean photon number is also plotted for clarity, indicating that the Zener tunneling hardly change the photon number.

The excited electron can create photons via transition to the lower subband with photoemission, and mean photon number increases in the next stage. Therefore the intersubband transition with photoabsorption (and emission) is allowed, dominating the temporal evolution of $\langle \hat{S}_z \rangle$, and there we can not observe the Zener tunneling.

After a while, the mean photon number gradually decrease thanks to Zener tunneling to a lower subband and subsequent photoabsorption. And then the transition via photoabsorption is prohibited again and the Zener tunneling appears markedly, as shown in Fig. 9. The temporal evolution of electronic inversion continues this cycle thereafter.

Generally, under the resonant condition given in Eqs. (26) and (28), we can observe the Zener tunneling when the mean photon number is relatively smaller than $\Delta_0/\hbar\omega$, and, if the photon number is greater than it, the photoabsorption (and emission) dominates the intersubband transition in the time domain. By using quantized photon field instead of the classical one, we can sweep the two kinds of intersubband transition.

5 Summary

In this Paper, we have described the external dc biased superlattice interacting with a single-mode quantized photon field. Under some approximations, the time development operator is equivalent to either one of the displacement operator $\hat{D}(\alpha)$, the QPA squeezing operator $\hat{S}(\xi)$, or the optical Kerr operator $\hat{U}_{\mathrm{K}}(\gamma)$ under the single subband condition. We can easily control the corresponding quantized photon states by the external dc bias. Even for the case of finite intersubband transition rate, which reduces the controllability, the scheme is still possible with use of the best set of parameters. Thus it offers a method for generation of nonclassical photon states without having recourse to usual optical nonlinear materials.

Finally, we would like to mention the analogy with Josephson-Junction [15] driven by constant dc current. By replacements $\Delta_0/2$, Ω_{B0}, and Ω_{B1} with $-E_{\mathrm{J}}$, $I_0/2e$, and $I_1/2e$ in Eq. (10) respectively, we can obtain the interaction Hamiltonian between single-mode quantized photon field and tunneling Cooper pairs. (Where E_{J}, I_0, and I_1 are Josephson coupling energy, external dc current, and alternating current per photon respectively.) The scheme also has a fine controllability of quantized photon field and can emit nonclassical light.

References

[1] See, e.g., P. Meystre and M. Sargent III, *Elements of Quantum Optics* (Springer-Verlag, Berlin, 1991); D. F. Walls and G. J. Milburn, *Quantum Optics* (Springer-Verlag, Berlin, 1994).

[2] F. Bloch, Z. Phys. **52**, 555 (1928).

[3] C. Zener, Proc. R. Soc. London Ser. A **145**, 523 (1934).

[4] See, e.g., F. Rossi, *Theory of Transport Properties of Semiconductor Nanostructures*, edited by E. Schöll (Chapman and Hall, London, 1997).

[5] J. Zak, Phys. Rev. Lett. **71**, 2623 (1993).

[6] X-G. Zhao, G. A. Georgakis, and Q. Niu, Phys. Rev. B **54**, R5235 (1996).

[7] For a review, see M. Nakayama, *Optical Properties of Low-Dimensional Materials*, edited by T. Ogawa and Y. Kanemitsu (World Scientific, Singapore, 1995), Chap. 3; G. Bastard, J. A. Brum, and R. Ferreira, *Solid State Physics* **44**, (Academic Press, Boston, 1991).

[8] T. Fukuo, T. Ogawa, and K. Nakamura, Phys. Rev. A **57**, 1367 (1998).

[9] M. Kitagawa and Y. Yamamoto, Phys. Rev. A **34**, 3974 (1986).

[10] The coupling constant of $\hat{b}_n \hat{c}_m^\dagger$ are greater than $\hat{b}_n \hat{c}_{m+1}^\dagger$ as much as 10^3 order in typical superlattice parameters, see ref. [11].

[11] A. Wacker, *Theory of Transport Properties of Semiconductor Nanostructures*, edited by E. Schöll (Chapman and Hall, London, 1997), Chap. 10.

[12] E. T. Jaynes and F. W. Cummings, Proc. IEEE **51**, 89 (1963); Review of the Jaynes-Cummings model was published by B. W. Shore and P. L. Knight, J. Mod. Optics **40**, 1195 (1993).

[13] M. Holthaus, Phys. Rev. Lett. **69**, 351 (1992).

[14] J. Rotvig, A.-P. Jauho, and H. Smith, Phys. Rev. Lett. **74**, 1831 (1995); J. Rotvig, A.-P. Jauho, and H. Smith, Phys. Rev. B **54**, 17691 (1996).

[15] See, e.g., A. Barone and G. Paternò, *Physics and Applications of the Josephson Effect* (Johon Wiley & Sons, New York, 1982).
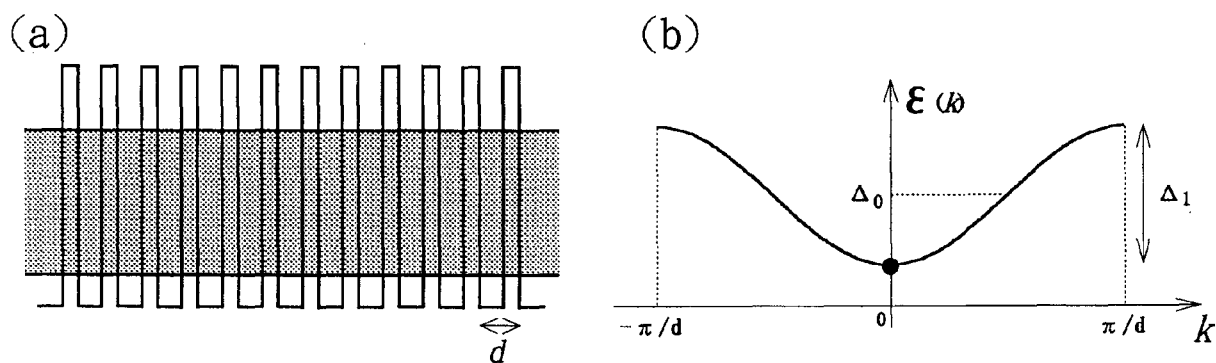
Figure 1: Subband dispersion of conduction electrons: (a) real space; (b) wave number space.
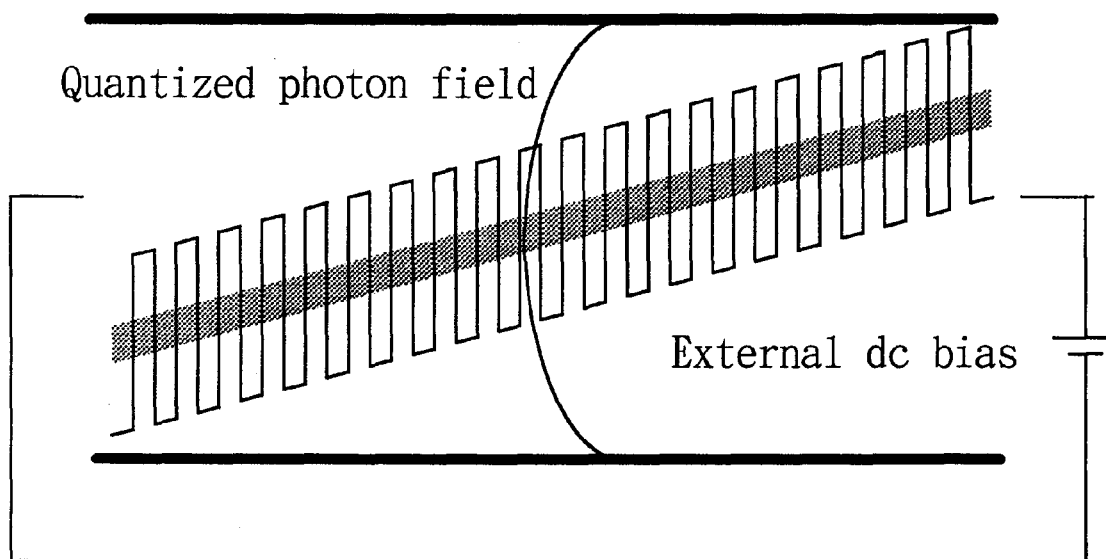

Figure 2: Schematical illustration of our system. The conduction electrons in semiconductor superlattice interacts with external dc electric field and single-mode quantized photon field.
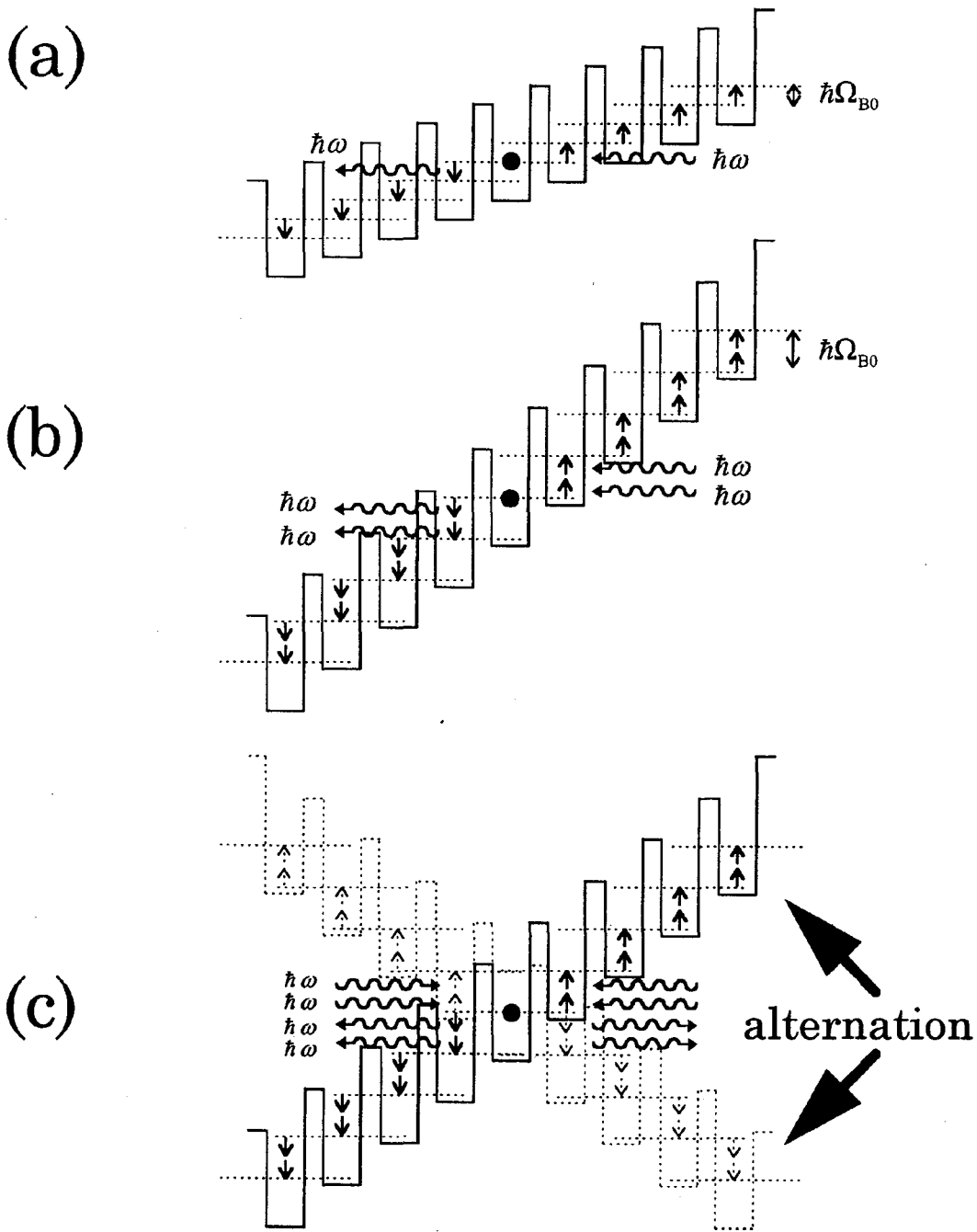
Figure 3: Illustration of the electron motion in an infinite superlattice due to photon emission (and absorption): (a) $\Omega_{B0} = \omega$ case; (b) $\Omega_{B0} = 2\omega$ case; (c) $\Omega_{B0} = 0$ case. The effect of external dc bias is described by a stairwise function for simplicity.
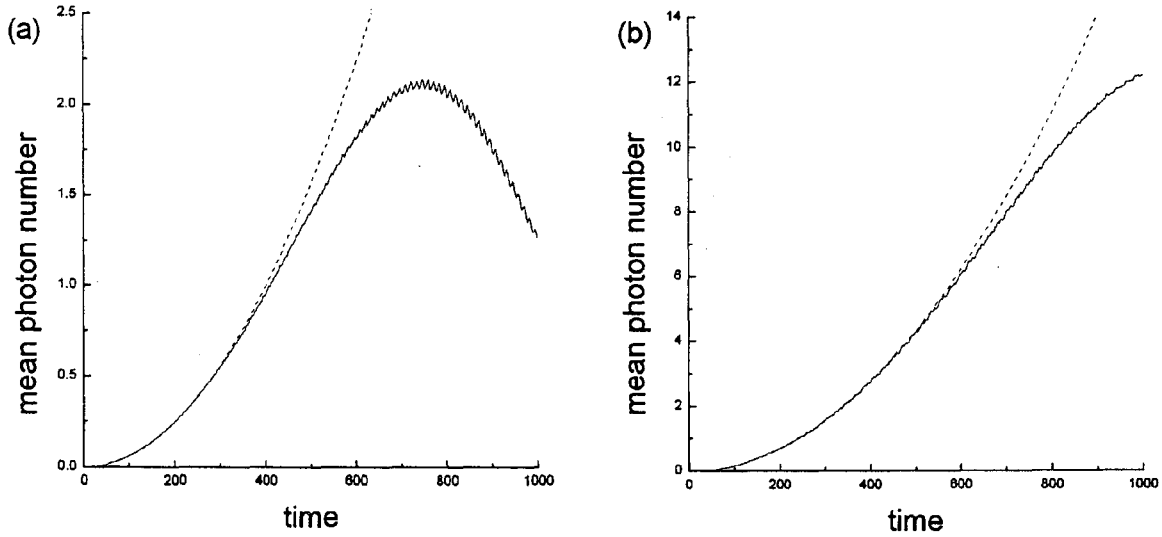
Figure 4: Time evolution of mean photon number in case of $\Omega_{B0} = \omega$: $\langle \hat{n} \rangle$ is plotted as a function of a normalized time $t' = \Delta_0 t/\hbar$ for (a) $\hbar\omega/\Delta_0 = \hbar\Omega_{B0}/\Delta_0 = 0.5$; (b) $\hbar\omega/\Delta_0 = \hbar\Omega_{B0}/\Delta_0 = 0.3$. Initial state at $t' = 0$ is the vacuum state $|0\rangle$ for the photon part and the lower subband $| \downarrow \rangle$ for electron part. Numerical parameters are chosen as $\hbar\Omega_{B1}/\Delta_0 = 0.1$, $\Delta_1/\Delta_0 = 0.1$, and $\hbar g_0/\Delta_0 = \hbar g_1/\Delta_0 = \hbar g_2/\Delta_0 = \hbar g_3/\Delta_0 = 0.01$.
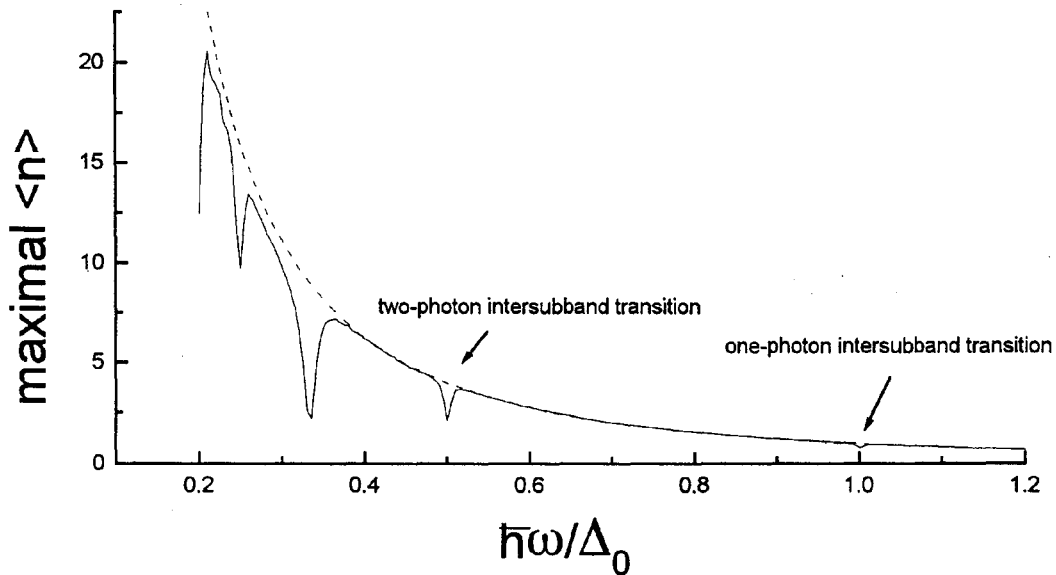
Figure 5: Maximal value of mean photon number $\langle \hat{n} \rangle$ during temporal evolution versus matching ratio $\hbar\omega/\Delta_0$ $(= \hbar\Omega_{B0}/\Delta_0)$. Numerical parameters are the same as in Fig. 4. Dashed line corresponds to the calculation without intersubband transition $(g_{0,1,2,3} = 0)$. (In the figure, the numerical calculations of temporal evolution are terminated at a proper t'.)
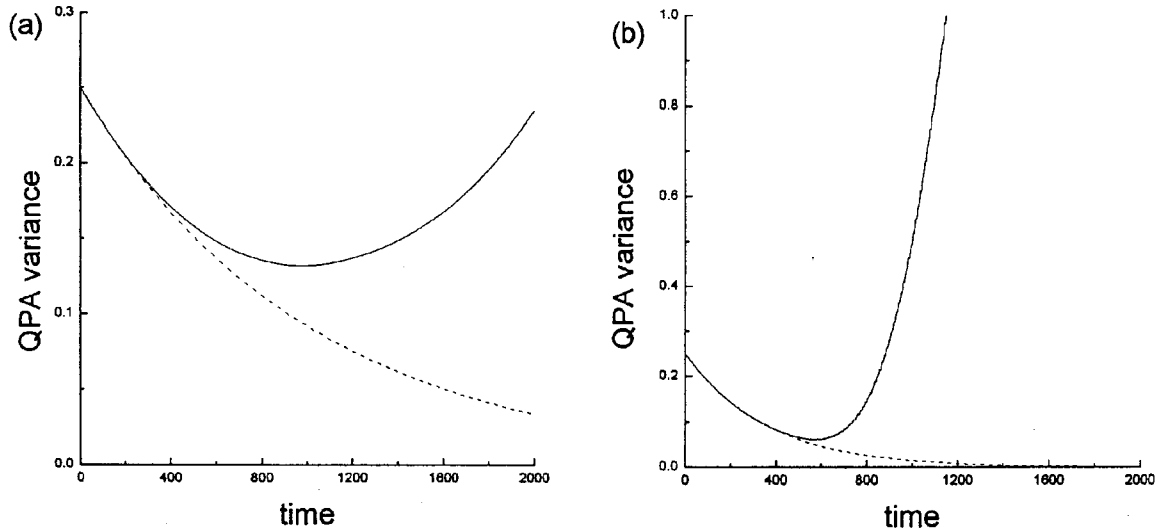
Figure 6: Time evolution of QPA variance in case of $\Omega_{B0} = 2\omega$ case: $\langle \Delta \hat{q}^2 \rangle$ is plotted as a function of a normalized time $t' = \Delta_0 t/\hbar$ for (a) $\hbar\omega/\Delta_0 = \hbar\Omega_{B0}/2\Delta_0 = 0.5$; (b) $\hbar\omega/\Delta_0 = \hbar\Omega_{B0}/2\Delta_0 = 0.3$. Initial state at $t' = 0$ is the vacuum state $|0\rangle$ for the photon part and the lower subband $| \downarrow \rangle$ for electron part. Numerical parameters are chosen as $\hbar\Omega_{B1}/\Delta_0 = 0.1$, $\Delta_1/\Delta_0 = 0.1$, and $\hbar g_0/\Delta_0 = \hbar g_1/\Delta_0 = \hbar g_2/\Delta_0 = \hbar g_3/\Delta_0 = 0.01$.
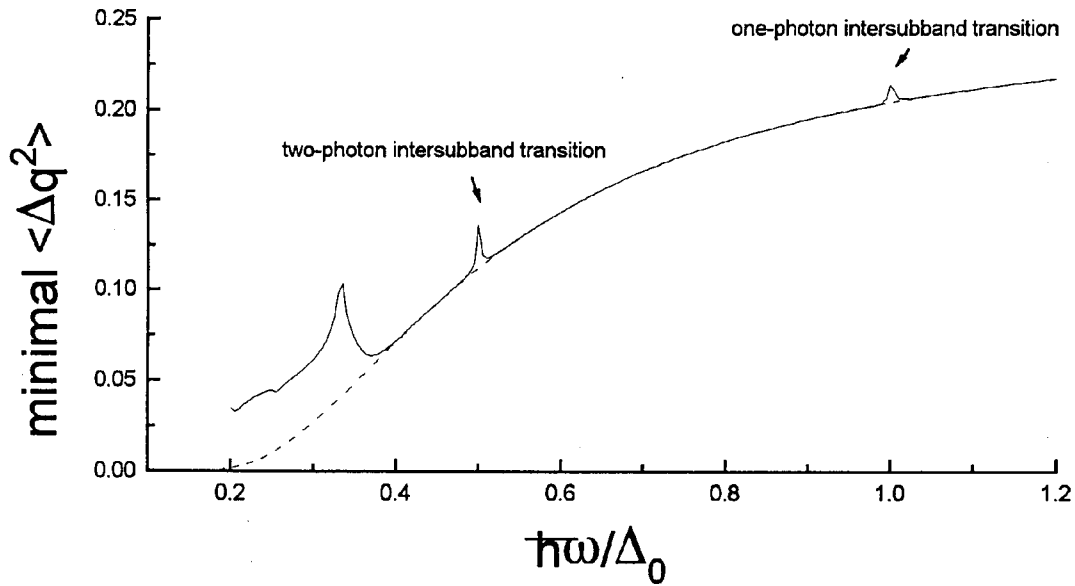

Figure 7: Minimal value of QPA variance $\langle \Delta \hat{q}^2 \rangle$ during temporal evolution versus matching ratio $\hbar\omega/\Delta_0$ $(= \hbar\Omega_{B0}/2\Delta_0)$. Numerical parameters are the same as in Fig. 6. The Dashed line corresponds to the calculation without intersubband transition $(g_{0,1,2,3} = 0)$. (In the figure, the numerical calculations of temporal evolution are terminated at a proper t'.)
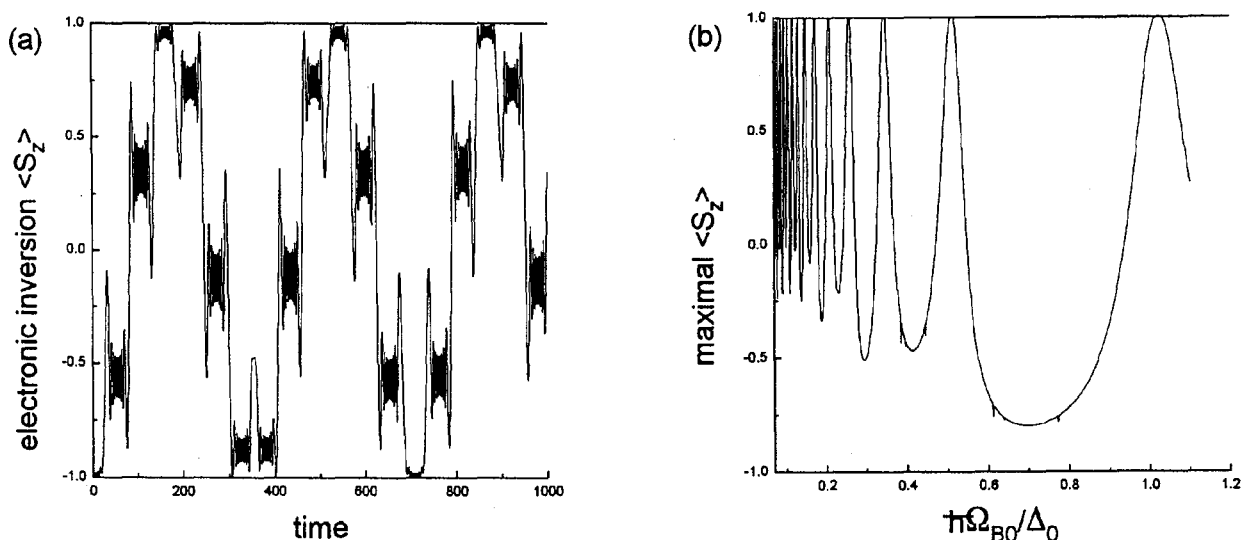
Figure 8: (a) Time evolution of electronic inversion in the ninth Zener resonance case: $\langle \hat{S}_z \rangle$ is plotted as a function of a normalized time $t' = \Delta_0 t/\hbar$. Initial state at $t' = 0$ is the lower subband $| \downarrow \rangle$ for electron part. Numerical parameters are chosen as $\hbar\Omega_{B0}/\Delta_0 = 0.115686, \hbar\Omega_{B1}/\Delta_0 = 0$, $\Delta_1/\Delta_0 = 18.0$, $\hbar g_0/\Delta_0 = 0.1$, and $g_{1,2,3} = 0$. (b) Maximal value of electronic inversion $\langle \hat{S}_z \rangle$ during temporal evolution versus matching ratio $\hbar\Omega_{B0}/\Delta_0$. Numerical parameters are the same as in (a). (In the figure, the numerical calculations of temporal evolution are terminated at a proper t'.)
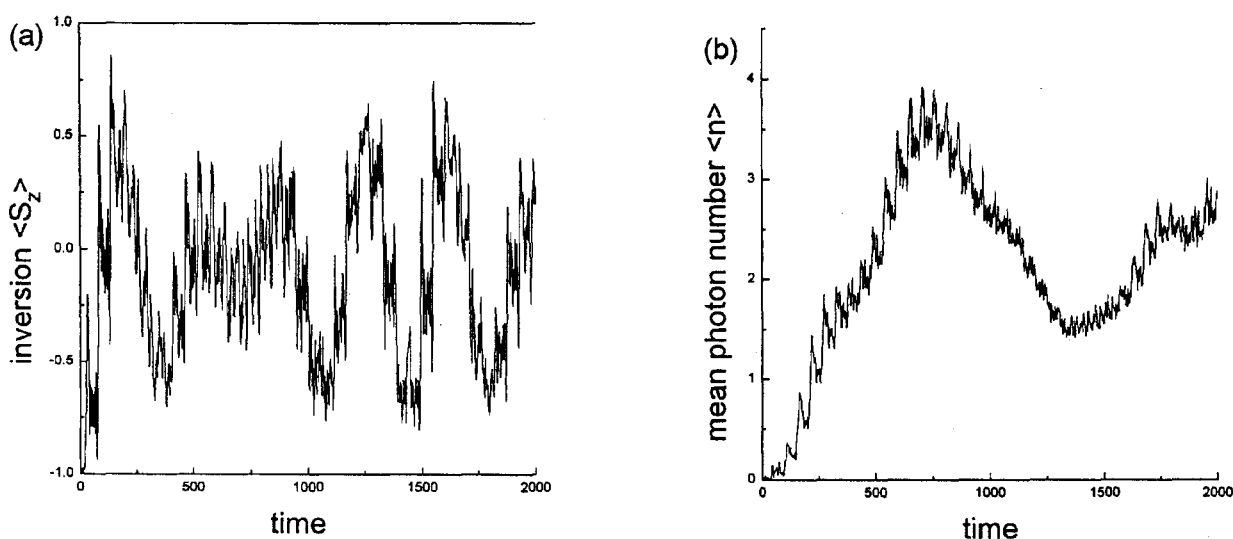

Figure 9: Time evolution of (a) electronic inversion and (b) mean photon number in the ninth Zener resonance case: $\langle \hat{S}_z \rangle$ and $\langle \hat{n} \rangle$ are plotted as a function of a normalized time $t' = \Delta_0 t/\hbar$, respectively. Initial state at $t = 0$ is the vacuum state $|0\rangle$ for the photon part and the lower subband $| \downarrow \rangle$ for electron part. Numerical parameters are chosen as $\hbar\omega/\Delta_0 = 0.5$, $\hbar\Omega_{B0}/\Delta_0 = 0.115686$, $\hbar\Omega_{B1}/\Delta_0 = 0.1$, $\Delta_1/\Delta_0 = 18.0$, $\hbar g_0/\Delta_0 = 0.1$, and $\hbar g_1/\Delta_0 = \hbar g_2/\Delta_0 = \hbar g_3/\Delta_0 = 0.01$.